the FEBS Journal

Structural determination of the phosphorylation domain of the ryanodine receptor

Parveen Sharma[1], Noboru Ishiyama[2], Usha Nair[1,3], Wenping Li[1], Aiping Dong[1,3], Tetsuaki Miyake[1], Aaron Wilson[1], Tim Ryan[1], David H. MacLennan[4], Thomas Kislinger[2,5], Mitsuhiko Ikura[2,5], Sirano Dhe-Paganon[1,3,*] and Anthony O. Gramolini[1]

1 Department of Physiology, University of Toronto, Ontario, Canada
2 Campbell Family Cancer Research Institute, Ontario Cancer Institute, Princess Margaret Cancer Center, University Health Network, Toronto, Ontario, Canada
3 Structural Genomics Consortium, University of Toronto, Ontario, Canada
4 Banting and Best Department of Medical Research, University of Toronto, Ontario, Canada
5 Department of Medical Biophysics, University of Toronto, Ontario, Canada

Keywords
excitation contraction; malignant hyperthermia; phosphorylation site; RyR; X-ray crystallography

Correspondence
A. Gramolini or S. Dhe Paganon, Department of Physiology, University of Toronto, Ontario M5S 1A8, Canada
Fax: +1 416 978 8528
Tel: +1 416 978 5609
E-mail: anthony.gramolini@utoronto.ca; dhepag@gmail.com

***Present address**
Division of Nephrology, Children's Hospital Boston, Harvard Medical School, Boston, MA, USA
Fax: +1 617 407 1475
Tel: +1 617 407 1900

(Received 9 July 2012, revised 13 August 2012, accepted 15 August 2012)

doi:10.1111/j.1742-4658.2012.08755.x

The ryanodine receptor (RyR) is a large, homotetrameric sarcoplasmic reticulum membrane protein that is essential for Ca^{2+} cycling in both skeletal and cardiac muscle. Genetic mutations in RyR1 are associated with severe conditions including malignant hyperthermia (MH) and central core disease. One phosphorylation site (Ser 2843) has been identified in a segment of RyR1 flanked by two RyR motifs, which are found exclusively in all RyR isoforms as closely associated tandem (or paired) motifs, and are named after the protein itself. These motifs also contain six known MH mutations. In this study, we designed, expressed and purified the tandem RyR motifs, and show that this domain contains a putative binding site for the Ca^{2+}/calmodulin-dependent protein kinase β isoform. We present a 2.2 Å resolution crystal structure of the RyR domain revealing a two-fold, symmetric, extended four-helix bundle stabilized by a β sheet. Using mathematical modelling, we fit our crystal structure within a tetrameric electron microscopy (EM) structure of native RyR1, and propose that this domain is localized in the RyR clamp region, which is absent in its cousin protein inositol 1,4,5-trisphosphate receptor.

Database
The crystal structure of the RyR1 phosphorylation domain (amino acid residues 2734–2940) has been submitted to the Protein Data Bank under accession number 3RQR.

Structured digital abstract
- **RyR1 C3** physically interacts with **CaMKIIβ** by pull down (View interaction)
- **RyR1 C3** binds to **CaMKIIβ** by pull down (View interaction)
- **CaMKIIβ** physically interacts with **RyR1 C3** by anti tag coimmunoprecipitation (View Interaction: 1, 2)

Abbreviations
EM, electron microscopy; CaMK, calcium/calmodulin-dependent protein kinase; GFP, green fluorescent protein; IP_3, inositol 1,4,5-trisphosphate; IP_3R, inositol 1,4,5-trisphosphate receptor; IP_3R-SD-IBC, IP_3R-suppressor domain-IP_3 binding core; MH, malignant hyperthermia; RyR1, ryanodine receptor 1.

Introduction

The ryanodine receptor is a large, homotetrameric sarcoplasmic reticulum membrane protein that is an essential component of Ca^{2+} cycling in both skeletal and cardiac muscle. In skeletal muscle, excitation–contraction begins with depolarization of sarcolemmal and transverse tubular membranes, triggering a conformational change in the dihydropyridine receptor and ryanodine receptor type 1 (RyR1), leading to Ca^{2+} release from the sarcoplasmic reticulum via RyR1 and generation of skeletal muscle contraction. Relaxation is then initiated by re-uptake of intracellular Ca^{2+} through the action of the sarco/endoplasmic reticulum Ca^{2+}-ATPase type 1 [1,2]. Correct functioning of the contraction/relaxation cycle relies on a precise balance between Ca^{2+} release and re-uptake. Disruptions in this balance, such as those that result from mutations in the proteins involved in the Ca^{2+} uptake and release processes, lead to muscle diseases, including malignant hyperthermia (MH) and central core disease, two conditions that arise from abnormalities in RyR1 [3–5]. MH is a pharmacogenetic disorder of skeletal muscle that is triggered in susceptible individuals by inhalational anaesthetics and depolarizing skeletal muscle relaxants [3,5]. Susceptible individuals respond with skeletal muscle rigidity, tachycardia, unstable and rising blood pressure, and eventually dramatic hyperthermia. Central core disease is an autosomal dominant myopathy that is characterized by hypotonia during infancy, proximal muscle weakness, delayed motor development, and reduced muscle bulk [4,5].

Three isoforms of the ryanodine receptor have been identified: RyR1 is predominantly expressed in skeletal muscle, RyR2 is mainly expressed in cardiac tissue, and RyR3 is expressed ubiquitously [2,6,7]. All three isoforms comprise four identical subunits of approximately 5000 amino acids. With a total molecular mass of approximately 2 million Daltons, the homotetrameric ryanodine receptor is the largest known Ca^{2+} channel [2,8]. Monomers comprise a large cytoplasmic region (residues 1–4300) and a transmembrane region that is predicted to contain six to eight transmembrane helices [9].

Analysis of the primary sequence of RyR1 revealed four repeats found as two closely associated pairs or two tandem motifs in all isoforms; the four repeats were termed RyR motifs or domains [9]. The linker between the second tandem motifs (residues 2725–2844 and 2845–2958) contains the major phosphorylation site of RyR1 (Ser2843) [10]. Mutations that give rise to MH and central core disease are clustered into three hotspots (region 1, Met1–Arg614; region 2, Arg2162–Arg2458; region 3, Leu4800–Glu4900), although mutations have been found throughout the RyR1 sequence including six MH mutations (E2764K, T2787S, R2840W [11,12], L2867G, E2880K and R2939K) in the region encompassing the known phosphorylation site.

The large size of this protein has made its structural analysis a challenge. Previous 3D cryo-EM structures to resolutions of up to approximately 9 Å revealed a very dynamic homotetramer structure for RyR1 [13–16]. Very recently, a high-resolution crystal structure of the N-terminal region (amino acids 1–599) of RyR1, coupled with cryo-EM mapping studies, suggested that homotetrameric interactions play critical functional roles [17,18]. By using affinity-tag purification of the large cytosolic domain of RyR1 coupled with LC-MS, we recently identified the calcium homeostasis endoplasmic reticulum protein as an integral membrane protein that binds to RyR1 [19], adding to the list of known integral membrane interacting partners of RyR1 including proteins such as the dihydropyridine receptor, junctin and triadin, and soluble proteins such as FK506 calmodulin, protein kinases and phosphatases [10,20,21]. Here, we employed a similar purification strategy to confirm binding of calcium/calmodulin-dependent protein kinase IIβ (CaMKIIβ) to this region, and provide a high-resolution crystal structure for the central region that contains the known phosphorylation site of RyR1 and six known human malignant hyperthermia disease mutations.

Results

Crystal structure of the domain containing the phosphorylation site

Sequence analysis of the C3 construct containing the known phosphorylation site showed a highly conserved region across species, with $\geq$ 75% sequence identity across all seven species and 98% sequence identity between rabbit and human RyR1 (Fig. S1), suggesting an essential role for either cellular viability and/or protein–protein interaction [22]. To generate functional hypotheses, we sought to determine the structure of the rabbit RyR domain. We designed, cloned and purified 25 nested loop constructs of the RyR domain, of which one construct (2734–2940) produced crystal hits in sodium citrate at pH 8.5 (see Experimental procedures). Upon optimization, crystals diffracted to 2.2 Å resolution (Table S1). The structure was solved

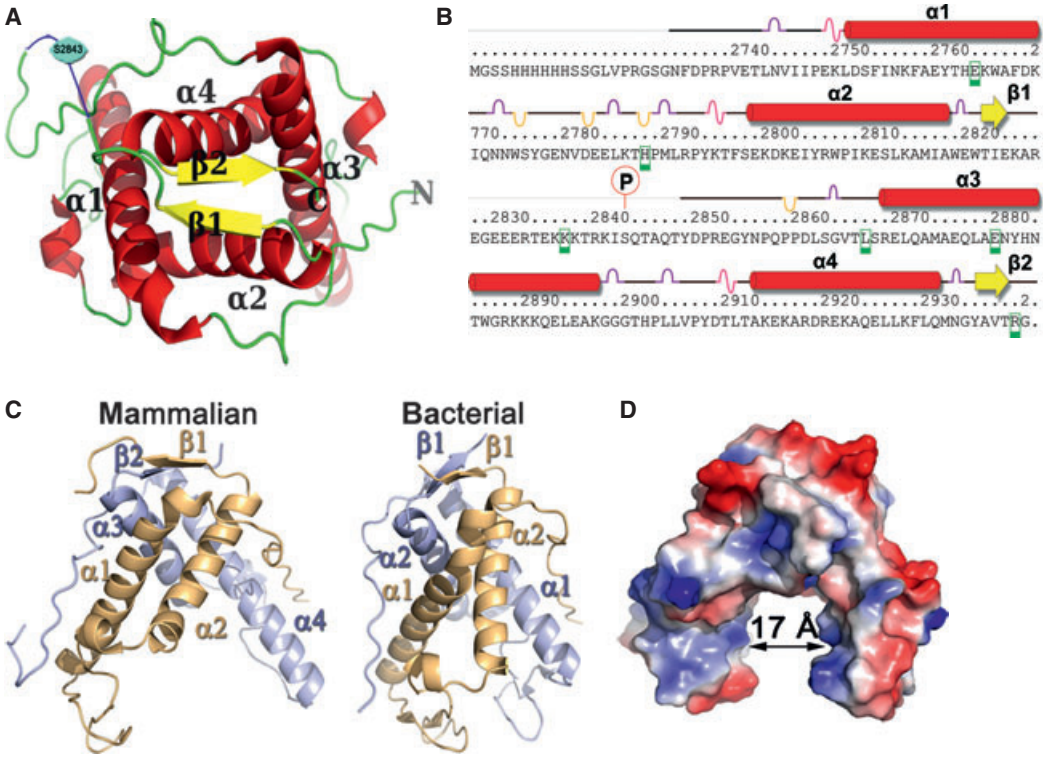

Fig. 1. Features of the RyR1 C3 construct crystal structure. (A) Ribbon diagram of rabbit the RyR1 C3 construct (residues 2734–2940) containing two repeating RyR domains. The two structural repeats are related by an approximate twofold symmetry. The structure is predominantly α-helical, with each repeat consisting of two α-helices (α1–α4, red), a β-sheet (β1 and β2, yellow) and intervening loop segments (green). The electron density for the residues between 2831 and 2848 was limited, and the structure was approximated from the limited data available in this region (blue). (B) Schematic of the sequence showing the exact regions of α1–α4 (red), β1 and β2 (yellow), 3_{10} helices (pink), and β bridge amino acids (gold) and turns (purple). The phosphorylation site Ser2843 is indicated. Green squares indicate the six MH mutations. (C) Comparison of our C3 crystal structure with the putative ryanodine receptor from *Bacteroides thetaiotaomicron* VPI-5482. The RyR repeats are shown individually as two RyR domain individual repeats (RyR domain 1 in gold and RyR domain 2 in grey) to facilitate comparison with the putative ryanodine receptor from *Bacteroides thetaiotaomicron* VPI-5482, which was crystallized as a monomer. (D) The surface charge distribution shows that the structure contains an outer positive area (red) and an inner negative area (blue), and that a 17 Å central cleft is formed by the four helices.

using single-wavelength anomalous scattering from sulfur atoms of methionine residues, and a model was built and refined using standard software (Fig. 1A, PDB ID 3RQR [23]). Resulting from two interwoven RyR elements, the domain comprised a four-helix bundle stabilized by a two-stranded β-sheet. Two helices (referred to as the legs) extended to a symmetrical upside-down U-shaped form (Fig. 1A,B). Each RyR motif contained two α-helices (α1–α4) and a β-strand; the helices were connected by a loop and a 3_{10} helix (Fig. 1B). Each RyR motif consists of a two-fold symmetrical structure in which α1, α2 and β1 make up one half and α3, α4 and β2 make up the second half. The linker connecting the two RyR motifs, which contained the known phosphorylation site (Ser2843), had limited electron density and was presumed to be mobile and dynamic. Weak electron density was observed for the backbone of approximately five residues of the 19-residue linker, and these unlabelled residues were included in the final model. The observation that the phosphorylated residue was within a 19-residue flexible linker (residues 2830–2849) supported the notion that the residue is a physiologically relevant phosphorylatable site. A stretch of basic residues just upstream of the phosphorylation site (KKKTRKISQ) suggested that the protein kinase responsible for this activity is a member of the basophilic serine/threonine kinase group, which includes protein kinase A, alpha serine/threonine-protein kinase (AKT) and CaMK [24].

A Dali search [25] revealed one PDB hit of significance, a protein of unknown function from one of the dominant intestinal microbiota, *Bacteroides thetaiotaomicron* VPI-5482 (PDB ID 3NRT). Interestingly, although the bacterial gene encoded one RyR domain,

the structure revealed a homodimer. Structural comparison showed a conserved overall fold comprising two long, right-handed α-helices that packed with an identical molecule in the asymmetric unit to create a bi-lobed arrangement similar to that seen in our structure (Fig. 1C). This suggested that, despite low primary amino acid sequence similarity between the bacterial and mammalian proteins (35% identity with the first RyR motif), the overall packing of these tandem motifs is probably quite important.

Interestingly, the 'feet' of the bacterial structure were bound together by a magnesium atom coordinated by aspartic acids, leaving a relatively large opening between the 'legs'. A surface representation of the rabbit RyR (Fig. 1D) revealed that the feet were unbound, but acidic residues did exist that may mediate similar interactions. The space between the two feet of the mammalian structure was approximately 17 Å from one side to the other, and may accommodate either small molecules or peptides.

Localization of the RyR domain of in cryo-EM maps of RyR1

We applied a modeling approach using the SITUS program package [26] to perform rigid-body mathematical placement of our 2.2 Å C3 crystal structure into the previously determined 10.2 Å cryo-EM structures of RyR1 in its open state (EMDB ID 1607) and closed state (EMDB ID 1606). We monitored the top solutions generated by the program, and identified two possible locations for the localization of the C3 crystal (Fig. S2). For the closed state, solutions 1–6 mapped to sub-region 3, whereas solutions 7–10 docked to sub-region 10. For the open state, solutions 1–8 mapped to domain 10, and solutions 9 and 10 mapped to domain 3 (Fig. S2). The low docking contrast of these solutions meant that both sub-regions were equally plausible locations for the RyR domain. However, this mathematical localization, coupled with previous studies has provided evidence to guide and support the structural fit of the C3 crystal into sub-region 10 in the clamp region of RyR1. Specifically, it was determined previously that the epitope of the RyR1 primary antibody 34C included amino acid residues 2756–2803 of RyR1 [27], corresponding to residues 2722–2769 of RyR2 that map to near sub-region 6 in the clamp domain of RyR2 [27,28], which is adjacent to our proposed binding domain 10, and a construct containing GFP after Tyr2801 localized to the bridge between domains 5 and 6 [27]. Therefore, although it is a low-resolution NMR structure and there is potential for errors in the antibody mapping, we propose that our crystal structure localizes in domain 10 of the 10.2 Å cryo-EM structures of RyR1 (Fig. 2A–C). After deposition of our structure into the PDB database, an independent study also crystallized the phosphorylation region (2734–2940) of RyR1 and proposed the structural fit into domain 10, although they too emphasis ambiguity when docking this structure and provide multiple solutions of docking into the cryo-EM open structure [29]. In order to obtain insight into the dynamic changes that accompany channel gating, we examined differences between the open and closed states (Fig. 2D). Superposition of RyR1 in the open state (blue ribbon with grey envelope) and closed state (red ribbon with pink envelope) suggested that some of the most prominent changes occur in the clamp region during gating, which may be described as a downward shift of domains 10, 7 and 8a (indicated by the arrow in Fig. 2D and Movie S1) upon channel opening, in agreement with previous studies [16,30]. These observations suggested that this RyR domain is highly dynamic and either influences or is influenced by channel opening and closing. Interestingly, in comparison to the open state, the RyR domain fitted in the closed state is rotated approximately 180° about its pseudo-twofold axis, with the phosphorylation site pointing outward (Fig. 2D).

Disease mutation mapping

The C3 crystal structure contained six known human MH mutations (E2764K [31], T2787S [32], R2840W [11,12], L2867G [31], E2880K [12] and R2939K [33]), the precise locations of which were analysed (Fig. 3). The R2840W mutation, which is three residues upstream of the phosphorylation site (Ser2843) and localized to the missing loop, may represent a disruption of the interaction with the basophilic serine/threonine kinase, and may be associated with decreased levels of phosphorylation at Ser2843. Interestingly, the E2764K and E2880K mutations not only have similar wild-type and mutant residues, they occurred on equivalent and symmetry-related and solvent-exposed regions of the protein and both sat within negatively charged patches. The E2764K mutation was located in α1 helix of the first RyR motif, and the E2880K mutation was located in the α3 helix in the second RyR motif. Equivalency suggested that these sites are involved in symmetric interactions, and charge reversal within negatively charged patches may disrupt protein–protein interactions. Although the Thr2787 side-chain hydroxyl was involved in a weak hydrogen bond with the backbone carbonyl group of Asn2780, the T2787S mutation is a conserved change and is unlikely to affect

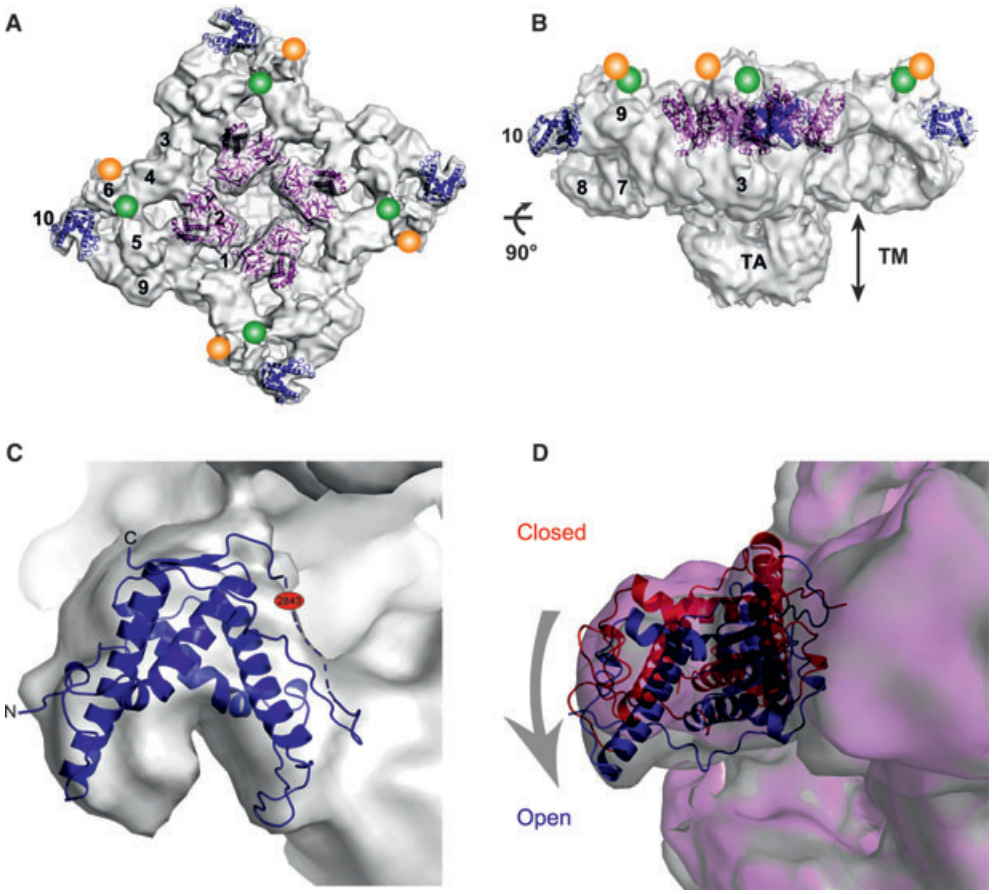

Fig. 2. Mapping of the C3 crystal structure into the cryo-EM map of RyR1. (A) Placement of the RyR domain into the cryo-EM map of the RyR1 tetramer (EMDB ID 1607) (grey) in the open state. The best solution placed the RyR domain (blue) in sub-region 10, which is localized approximately 75 Å away from the N-terminal ABC region (purple) that was previously positioned in sub-regions 1, 2a and 2b [18]. The previously determined locations of GFP inserted after Y2801 of RyR2 and the monoclonal antibody specific for residues 2756–2803 of RyR1 [27] are indicated by green and orange circles, respectively. Numbers indicate domain numbers. (B) Side view of the docked molecules. (C) Close-up view of the RyR domain docked in sub-region 10 showing the missing loop (residues 2831–2848) indicated by dashed line and the phosphorylation site shown in red that faces the centre of the tetramer but is located next to a cleft. (D) Placement of the RyR domain in the cryo-EM maps of RyR1 in the open state (blue ribbon with grey envelope) and closed state (red ribbon with pink envelope). In comparison to the open state, the RyR domain in the closed state is rotated approximately 180° about its pseudo-twofold axis, with the phosphorylation site pointing outwards.

possible hydrogen bonding interactions; how this mutation may affect the structure is unclear. Leu2867 is part of the core residues and probably stabilizes the conformational arrangement of the α3 (2869–2897) and α4 (2916–2933) helices and of an extended stretch of residues that bridged the two tandem domains. Mutation of this residue to glycine and the consequent absence of stabilizing hydrophobic interactions may affect the local and overall conformational flexibility and stability. The guanidinium group of Arg2939 formed bivalent interactions with two side chains from α3 (Glu2870 and Gln2877), and its mutation to lysine may disrupt these interactions and destabilize the fold. Based on our fitting of this region in the molecular volume generated by electron microscopy, Arg2939 may be a solvent-exposed residue forming part of an extended loop in the base of the structure, and its mutation may disrupt potential interaction with other proteins.

Comparison to RyR2 and RyR3

Amino acid sequence comparison between the RyR domain of RyR1 and the equivalent domain in RyR2 (2699–2907) showed 64% sequence identity, and comparison between RyR1 and the equivalent domain in RyR3 (2599–2804) showed 62% sequence identity between the paralogs (Fig. S3). Mapping divergent residues (grey) onto a surface representation of the C3

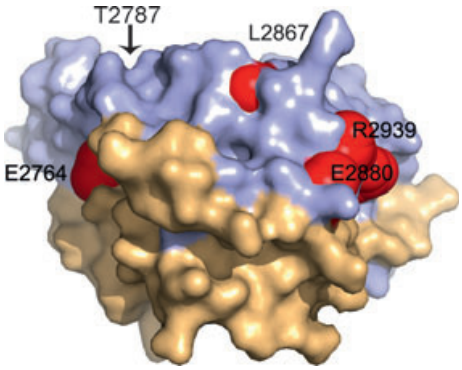

Fig. 3. Mapping of MH mutations into the C3 crystal structure. Mapping of the six known MH mutations onto our crystal structure shows that Glu2764, Glu2880, Thr2787 and Arg2939 are surface-exposed residues, whereas Leu2867, although somewhat exposed, fits into a cleft defined by residue side chains Q2924, L2927, K2928 and Q2931 and stabilizes the conformational arrangement of the α3 (2869–2897) and α4 (2916–2933) helices. Arg2840, which is three residues upstream of the phosphorylation site, localizes to the missing loop in our structure.

crystal RyR domain (Fig. 4A–D) indicated that the β-sheets, the surfaces of the α2 and α3 helices and the inner core of the structure were conserved. Divergence occurred in the α1 helix and in the loop region between α1 and α2 on one of the legs of the structure. Similarly, comparison amongst seven species (Fig. 4E, F and Fig. S3) also showed a conserved core; divergence occurred predominantly in the loop region between α1 and α2 on the left leg of the structure. These results are consistent with the notion that inner curvature of the RyR domain plays a functional role, possibly by binding ligands.

Comparison to the IP_3 receptor

Together with the RyR receptor, the inositol 1,4,5-trisphosphate receptor (IP_3R) represents the second principal channel responsible for mobilizing internal Ca^{2+}. IP_3Rs are large intracellular Ca^{2+} release channels that, like the RyR receptors, form homotetramers, and whose opening requires binding of the two intracellular messengers inositol 1,4,5-trisphosphate (IP_3) and Ca^{2+} [34]. The two receptors share considerable structural and functional homologies, and possess a similar basic architecture in the N-terminal region [17,35] and the transmembrane domain [34]. We superimposed the cryoEM structure of the IP3 receptor (EMDB ID 5278, yellow) and the cryoEM structure of RyR1 in the open state (grey), aligned by their N-terminal (NT) regions (using the high similarity between the NT domain of IP_3R-SD-IBC and RyR-ABC, the ABC domain of RyR) [18,36] (Fig. 5). Interestingly, the C3 crystal structure resides in the region located at a far protruded corner of the RyR structure (Fig. 5) that is not present in the IP3 receptor, suggesting that the proposed phosphorylation-dependent modulation of the gating function at this site is unique to the RyR function.

Binding of CaMKIIβ

CaMKII has been proposed previously to phosphorylate both RyR1 and RyR2 [2]. In order to confirm binding and determine the region specificity of binding, we cloned and amplified three constructs (C1–C3) (Fig. 6A) spanning various domains of the cytosolic region of RyR1 into the pET28a-LIC vector

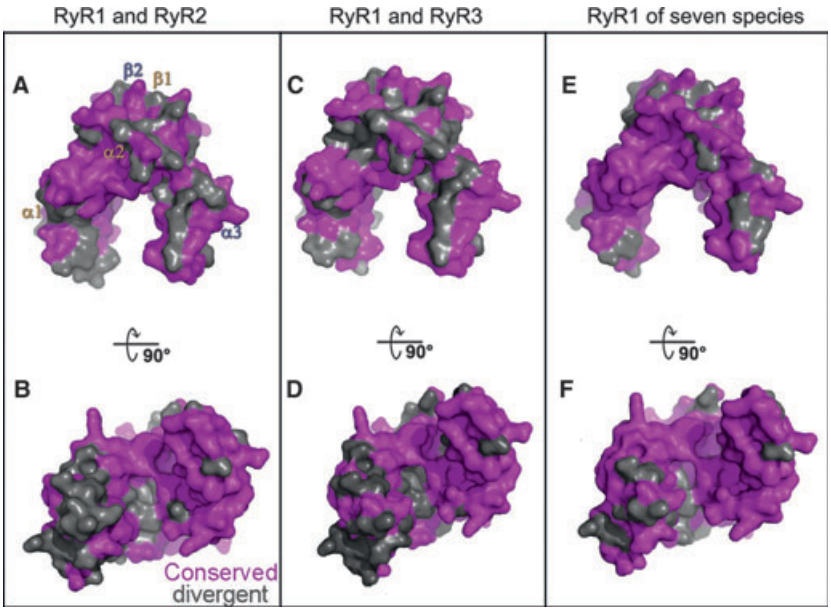

Fig. 4. Localization of conserved and divergent residues mapped onto a surface representation of the C3 crystal structure. (A) Residues that are divergent (grey) and conserved (pink) between RyR1 and RyR2. (B) Rotation of the image in (A) by 90°. (C) Residues that are divergent (grey) and conserved (pink) between RyR1 and RyR3. (D) Rotation of the image in (C) by 90°. (E) Residues that are divergent (grey) and conserved (pink) between RyR1 isoforms across seven species listed in Fig. S3. (F) Rotation of the image in (E) by 90°.

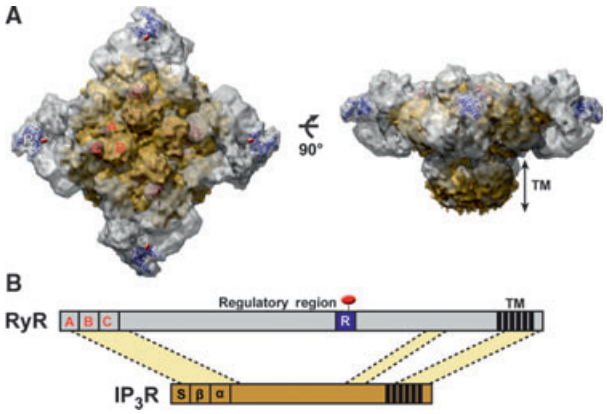

Fig. 5. Comparison of RyR1 and the IP_3 receptor. (A) Overlay of the cryo-EM maps of RyR1 (EMDB ID1607) (grey) and IP3R1 (EMDB ID 5278) (yellow) and the C3 crystal structure (blue). The red circle indicates the position of the Ser2843 phosphorylation site. (B) Scheme of the primary sequence alignment of RyR1 and IP_3R1. These proteins share 20–30% sequence identity in three conserved regions (light yellow). The RyR domain (blue box) is present within the regulatory region of RyR, but is not present in IP_3R1.

(GenBank vector accession number EF442785). Purification of the three constructs using His-link resin yielded highly enriched, purified levels of each protein at their respective molecular weights (Fig. 6B). The constructs were immobilized on His-link beads and incubated with mouse skeletal muscle lysate to allow formation of protein interaction complexes between the RyR1 constructs and *in vivo* binding partners. Mass spectrometry analysis showed that peptides that mapped to CaMKIIβ bound to the C3 construct but not to the C1 or C2 constructs (Table 1 and Table S2). To validate this interaction, we immobilized the C1–C3 constructs in the bacterial pET28a-LIC vector onto His-link beads. We purified CaMKIIβ cloned into the pEF-DEST51 Gateway vector, which contained dual V5 and six-histidine tags, over-expressed it in HEK-293 cells, and incubated this lysate with the immobilized C1–C3 constructs. The beads were then washed to remove non-specific binding, and western blot analysis of boiled beads showed that CaMKIIβ was bound only to the C3 construct when probed using the antibody against the V5 tag. The levels seen in the C1 and C2 western blots were nearly equivalent to the non-specific levels seen with empty beads (Fig. 6C). This data verified the mass spectrometry findings, and showed CaMKIIβ bound specifically to the C3 spanning region but not to the other constructs spanning the cytosolic region of RyR1. We further validated this interaction in a mammalian system by expressing RyR1 C3 in a mammalian vector containing an N-terminal FLAG tag (Fig. 6D), and incubating it with the cDNA for CaMKIIβ in the pEF-DEST51 Gateway vector. Cell lysates from HEK-293 cells transfected with FLAG-tagged C3 and V5/6xHis-tagged CaMKIIβ were subjected to immunoprecipitation experiments using antibody against the V5 tag. CaMKIIβ co-immunoprecipitated with C3 (Fig. 6D), but neither protein was detected in the A/G resin alone or the immunoglobulin control immunoprecipitations. Finally we examined the binding of CaMKIIβ to an S2843A-C3 phospho-deletion mutant. The S2843A mutant was expressed in a mammalian vector containing an N-terminal FLAG tag, and co-immunoprecipitated with V5/6xHis-tagged CaMKIIβ using an antibody against the FLAG tag. We found a reduction of approximately 20% in the amount of CaMKIIβ that co-immunoprecipitated with the S2843A phospho-deletion mutant compared to the wild-type C3 construct (Fig. 6E).

Discussion

The large size of the RyR protein has made its structural analysis a challenge. To overcome this challenge, we generated a high-resolution crystal structure of a smaller domain containing the known phosphorylation site at Ser2843. This revealed the fold of this poorly understood domain, and will provide the foundation necessary to elucidate the basis of interaction with binding partners and with other domains within the context of the full-length protein.

The clamp region of ryanodine receptors has been implicated as the likely site for tetramerization interactions [30,37], regulatory modulator interactions, and post-translational modifications [27,30]. Phosphorylation, for example, has been hypothesized to be an allosteric modulator of channel opening [30]. A comparison of RyR1 in the open and closed state shows that channel opening is associated with significant conformational changes of the cytoplasmic domain, particularly the clamp domains. Here, in keeping with the previous findings for this region in RyR2 [27] and the dynamic nature of the clamp region, we mapped the domain containing the known phosphorylation site of RyR1 to clamp region 10, and propose that it is a mobile structure that contains the phosphorylation site as well as the binding site of CaMKIIβ, which may in turn contribute to allosteric regulation.

In our RyR domain structure, disease-causing mutations fall within three categories: (a) mutations that may interfere with protein–protein interactions, including the solvent-exposed mutations E2764K, E2880K and R2939K, (b) mutations that probably disturb fold-

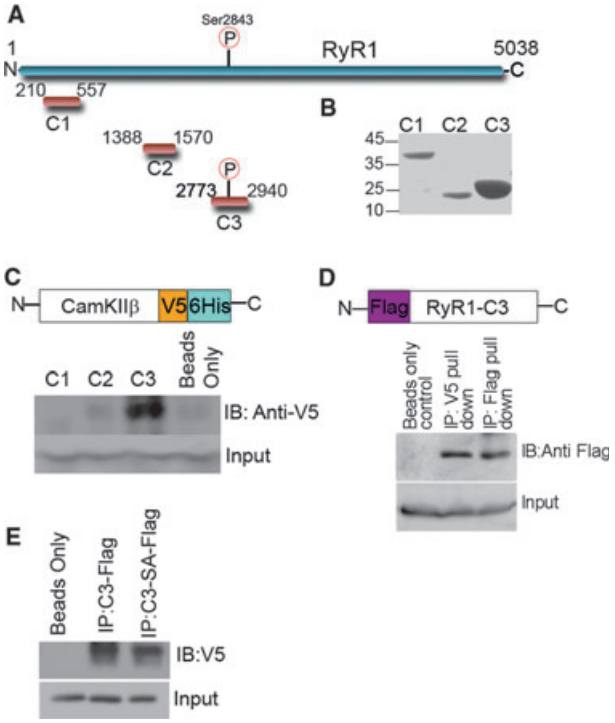

Fig. 6. CaMKIIβ binding to RyR. (A) Schematic showing constructs used for mass spectrometry analysis. (B) Coomassie gel of purified RyR1 constructs cloned into the pET28a-LIC vector shows enrichment of each construct at the correct molecular weight. (C) Schematic showing CaMKIIβ V5/6His constructs cloned into the pEF-DEST51 vector, and western blot of C1–C3 constructs incubated with V5/6His-tagged CaMKIIβ, showing binding with the C3 construct only. (D) Schematic showing the C3 mammalian construct containing an N-terminal FLAG tag used for immunoprecipitation and western blot analysis for confirmation of binding between C3 and CaMKIIβ. Cell lysates from HEK-293 cells transfected with FLAG-tagged C3 and V5/6His-tagged CaMKII were subjected to immunoprecipitation experiments using the antibody to the V5 tag. (E) Western blot analysis of binding of CaMKIIβ to the wild-type C3 construct and the C3S2843A mutant. Cell lysates from HEK-293 cells transfected with FLAG-tagged C3, FLAG-tagged C3S2843A and V5/6His-tagged CaMKIIβ were subjected to immunoprecipitation experiments using the antibody to the FLAG tag (RyR), and showed a 20% reduction of binding to the mutant compared to wild-type.

ing of this domain, including the L2867G mutation located between the α3 and α4 helices, and (c) mutations that may affect the affinity with upstream protein kinases, including R2840W. The last was of particular interest because this mutation is located in a dynamic loop three residues N-terminal to the known phosphorylation site [38,39]. In a systematic study using synthetic peptides to elucidate the minimal binding motif of CaMKII, a mutation at the Arg residue at position −3 from the phosphorylation motif, which is RXXS/T, where X is any residue [38,39], reduced the V_{max}/K_m of binding of CaMKII to the substrate by $\geq$ 300-fold [39], whereas mutations elsewhere in this motif had minimal effect on V_{max} or K_m. Therefore, the R2840W mutation disrupted the essential CaMKII binding motif and causes a reduction in phosphorylation of RyR1, the binding of regulatory modulators and ultimately the Ca^{2+} dynamics of RyR1. Similarly, disease-causing mutations within the recently solved crystal structure of the N-terminal domain of RyR1 (residues 1–559) were classified into three groups: (a) those that destabilized interfaces between the three N-terminal domains, (b) those that disturbed folding of individual domains, and (c) those that affected interfaces between neighbouring domains within the receptor [18]. A recent independent study by the same group resolved the crystal structure of the E2764K MH mutant, and confirmed our hypothesis that this mutation predominantly affects protein–protein interactions, as the structure revealed only a minor shift in neighbouring residues and the main effect was the alteration of the surface charge. Yuchi *et al.* were unable to resolve the crystal structure of L2867G and showed its decreased stability by thermal destabilization, which further confirms our view that this mutation located between the α3 and α4 helices probably causes unfolding of the domain, thereby destabilizing the crystal [29]. Taken together, these studies provide a framework for understanding the basis of the disease-associated mutations in this region of RyR1.

The structural and functional similarities between the RyR receptors and the IP_3 receptors probably reflect a common evolutionary origin [35]. However, the lack of the clamp region in the IP_3 receptor suggests that this region, in which our C3 crystal fragment was docked, is probably involved in regulating either a functional or protein interaction that is unique to RyR. These unique functions may include differences recently reported in smooth muscle cells, which found that RyRs underlie Ca^{2+} sparks, contribute to Ca^{2+} waves, and participate in the negative feedback regulation of myogenic tone in feed arteries but not downstream arterioles. In contrast, the IP_3Rs were found to contribute to Ca^{2+} waves and myogenic tone through a positive feedback mechanism in both feed arteries and their downstream arterioles [40].

CaMKII was shown to phosphorylate Ser2843 in RyR1 [2,41] and also Ser2814 in the equivalent region in RyR2 [42,43]. A comparison between the C3 regions in RyR1, RyR2 and RyR3 revealed that this region is highly homologous between the isoforms, and that the main area of divergence is in the loop regions between helices that maintain the structural integrity of the identified α-helices and the inner core structure. These data

Table 1. Number of CaMKIIβ peptides found in each mass spectrometry run for RyR1 C1–C3 constructs. The constructs were immobilized on His-link beads and incubated with mouse skeletal muscle lysate to allow formation of protein interaction complexes between the RyR1 constructs and *in vivo* binding partners. Control spectra were obtained from beads incubated with skeletal muscle lysate only. All experiments were run in triplicate (ND, none determined), and numbers in parentheses are total spectra for the specific peptide.

		Number of spectra			
Construct	Peptides	Total	*Run 1*	*Run 2*	*Run 3*
C1	ND	0	0	0	0
C2	AGAYDFPSPEWDTVTPEAK (1)	1	0	0	1
C3	LHDSISEEGFHYLVFDLVTGGELFEDIVAR (15) NLINQMLTINPAK (1) ESSDSTNTTIEDEDAK (1)	17	4	8	5

imply that the conserved residues are critical to the structure and function of this domain in the two isoforms, and that they may be involved in binding of RyR and CaMKII. These findings are of critical interest as CaMKII has been shown to be up-regulated and more active in congestive heart failure [44,45], a leading cause of mortality and morbidity worldwide with 50% of patients dying of sudden death syndrome attributed to ventricular arrhythmias [46]. Increased CaMKII-dependent phosphorylation of RyR2 appears to promote the development of ventricle arrhythmias, whereas inhibition of CaMKII phosphorylation of RyR2 prevents ventricular arrhythmias in mice with heart failure [45,47]. The current RyR crystal structure also allows us to predict and model the interaction between RyR2 and CaMKIIβ; however, generation of a co-crystal structure of RyR together with CaMKIIβ enables possible development of pharmacological targets that may be used to modify this interaction and provide new avenues for treating ventricular arrhythmias.

The crystal structure elucidated in this study provided structural insight into understanding the interaction, binding and conformational changes that may occur in RyR1 during channel opening and closing, and how this region may be regulated by the known phosphorylation site. Interestingly, localization of the C3 crystal in the open state showed orientation of the phosphorylation domain facing the centre of the tetramer; however, we showed that the C3 crystal has a 17 Å space between the two 'legs' that may accommodate either small molecules or peptides of CaMKIIβ. It was also noted that, when the C3 crystal structure is docked to the cryo-EM RyR structure domain in the closed state, it is rotated approximately 180° about its pseudo-twofold axis with the phosphorylation site pointing outwards, and further investigations are necessary to determine which of these solutions is correct.

Following the release of our C3 crystal structure [23], an independent group crystallized the phosphorylation domain of the ryanodine receptors [29]. Their crystal structure is in agreement with ours, and they also tentatively dock the crystal to domain 10 in the cryo-EM structure of RyR1. Further, our study found that this region binds to CaMKIIβ and that mutations of the known phosphorylation site (S2843A) caused a modest decrease in the ability of CaMKIIβ to bind to the region. Based on their phosphopeptide identification, Yuchi *et al*. identify up to four additional sites in this region that are potentially phosphorylated by CaMKII, which may explain why CaMKIIβ remains associated with this domain even though the Ser2843 site is unavailable in our model. Together, these studies increase our knowledge of a key regulatory domain in RyR receptors that can carry human disease mutations, although further progress will require in-depth analysis of neighboring domains, and how they affect or are affected by the architecture and movement of this small dynamic region in the open and closed state.

Experimental procedures

Cloning, expression and purification of the RyR1 construct

We designed, cloned and purified 25 nested-loop constructs of the rabbit RyR domain. Soluble constructs were screened using 192 sparse-matrix crystallization conditions, and one construct C3 (2734–2940) produced crystal hits. Two additional constructs located upstream of the phosphorylation region in RyR were referred to as C1 (804–1067) and C2 (1388–1570). These two constructs showed a high yield in purification but did not crystallize and were later used as negative controls to prove domain-specific binding of CaMKIIβ. All constructs were cloned into the pET28a-LIC expression vector (GenBank vector accession number EF442785) using an In-Fusion CF Dry-Down PCR cloning kit (Clontech, Mountain View, CA, USA). Competent BL21 (DE3) cells (Invitrogen, Burlington, ON, Canada) were transformed and grown using the LEX system (HarbingerBiotech, Toronto, ON, Canada) at 37 °C in

1 L bottles containing 900 mL terrific broth (Sigma, Oakville, ON, Canada) supplemented with 150 mM glycerol, 100 μM kanamycin and 600 μL antifoam 204 (Sigma). When the attenuance reached approximately 6.0, the temperature was reduced to 15 °C, and 1 h later, the culture was induced using 1 mM isopropyl thio-β-D-galactoside (BioShop, Burlington, ON, Canada) and incubated overnight (16 h) at 15 °C. The protein was purified by the Streamline purification method using His-link resin (Promega, Madison, WI, USA) as described previously [48]. The resin was washed four times 10 mins each using 10 mL of wash buffer (20 mM Tris pH 8.0, 500 mM NaCl, 20 mM imidazole pH 8.0). Protein was eluted using 8 mL elution buffer (20 mM Tris pH 8.0, 500 mM NaCl, 500 mM imidazole pH 8.0), and dialysed overnight at 4 °C against 50 vol dialysis buffer (20 mM Tris pH 8.0, 200 mM NaCl, 5 mM dithiothreitol). The protein sample was concentrated using a 3 kDa molecular weight concentrator (Millipore, Etobicoke, ON, Canada) at 3500 ***g*** to a final value of 41 $mg \cdot mL^{-1}$. The protein yield was approximately 20 mg per litre of bacterial culture.

Crystallization

Crystals were grown at 18 °C in sitting- and hanging-drop plates (Hampton Research, Aliso Viejo, CA, USA) by mixing equal volumes of protein (41 $mg \cdot mL^{-1}$) and crystallization buffer (in-house buffer SGCB03 composed of 1.2 M sodium citrate, 100 mM Tris, pH 8.5). Crystals appeared in approximately 2 weeks. Suitable crystals were cryoprotected by immersion in well solution supplemented with 24% v/v ethylene glycol or by dipping in 100% paratone (Hampton Research) prior to flash freezing in liquid nitrogen.

Crystal structure determination and refinement

Two diffraction datasets were collected. One dataset was collected on the Rigaku FR-E^+ DW X-ray generator (The Woodlands, TX, USA) at an incident wavelength of 2.29 Å, and a second, high-resolution dataset was collected on the 19ID beamline at Advanced Photon Source (Argonne, IL, USA). All datasets were integrated and scaled using the HKL3000 program suite [49]. Diffraction data and processing statistics for the two datasets are shown in Table S1. The crystals belong to space group $P4_32_12$, and the structure was refined using cell parameters $a = 68.77$, $b = 68.77$, $c = 91.38$ and $\alpha = \beta = \gamma = 90°$ (from high-resolution data). The structure was solved by the sulfur single-wavelength anomalous dispersion method using the data collected on the FR-E^+ DW X-ray generator. The programs SHELX [50] and SOLVE/RESOLVE [51,52] were used to locate the sulfur sites and perform initial model building. The high-resolution data collected on the 19ID beamline at Advanced Photon Source were used for structure refinement. Iterative model building was performed using the graphics program Coot [53], and maximum-likelihood refinement was performed using Buster 2.8.0 [54]. Structure refinement statistics are shown in Table S1.

Computational placement of the phosphorylation domain

Rigid-body mathematical placement of the phosphorylation domain structure into approximately 10 Å cryo-electron microscopy density maps of RyR1 (EMDB-1606, 1607 and 1275) was implemented using the six-dimensional search procedure in the Situs package [26]. To enhance the fitting contrast, the Laplacian filter was applied, and the density corresponding to the transmembrane region was omitted from the search. Placement of the crystal structure of RyR1-ABC (PDB ID 2XOA) was also performed using the above procedure. The University of California, San Francisco (UCSF) Chimera package [55] was used to visualize the results of the density maps, as well as the comparison of cryo-EM maps of RyR1 and InsP3R1 (EMDB ID EMDB-5278).

Mass spectrometry

Gel-free shotgun sequencing of tryptic digests was performed essentially as described previously [19]. Briefly, individual samples were first loaded onto microcapillary fused-silica columns with an internal diameter of 75 μm, packed with 7 cm of reversed-phase C18 resin (Magic C18: Michrom Bioresources, Auburn, CA, USA). The columns were aligned using an LTQ linear ion trap mass spectrometer, and the peptides were eluted using a 2 h water/acetonitrile gradient and ionized via electrospray ionization. The tandem mass spectra generated were matched to peptide sequences in the human IPI protein sequence database (http://www.ebi.ac.uk/IPI) using the X!Tandem algorithm (http://gpmdb.thegpm.org/).

Co-immunoprecipitation and western blotting

Standard techniques were used to perform co-immunoprecipitation and western blotting as described previously [19,56]. The antibodies used were anti-V5 (Invitrogen) and anti-His (Abcam, Cambridge, MA, USA).

Acknowledgements

The authors would like to thank Vladimir Ignatchenko (Department of Medical Biophysics, University of Toronto, Ontario, Canada) for excellent bioinformatic support. M.I. is supported by the Heart and Stroke Foundation of Ontario and the Canada Research Chair program. This work was funded by the Canadian

Institutes of Health Research (MOP-84267 to A.O.G. and T.K. and MOP-3399 to D.H.M.), the Neuromuscular Research Partnership (JNM -123674 to AOG) the Heart and Stroke Foundation of Ontario (T-6281 to A.O.G.), an Early Research Award from the Ontario Ministry of Research and Innovation to A.O.G., and an unrestricted grant from Boehringer Ingelheim Canada. A.O.G., M.I. and T.K. are Canada Research Chairs, and A.O.G. was a New Investigator of the Heart and Stroke Foundation of Canada. T.R. held a Heart and Stroke/Richard Lewar Centre of Cardiovascular Excellence Studentship and a Margaret Santalo Fellowship from the University of Toronto. The Structural Genomics Consortium is a registered charity (number 1097737) that receives funds from the Canadian Institutes for Health Research, the Canadian Foundation for Innovation, Genome Canada through the Ontario Genomics Institute, GlaxoSmithKline, Karolinska Institutet, the Knut and Alice Wallenberg Foundation, the Ontario Innovation Trust, the Ontario Ministry for Research and Innovation, Merck & Co. Inc., the Novartis Research Foundation, the Swedish Agency for Innovation Systems, the Swedish Foundation for Strategic Research and the Wellcome Trust.

References

1 Nakai J, Sekiguchi N, Rando TA, Allen PD & Beam KG (1998) Two regions of the ryanodine receptor involved in coupling with L-type Ca^{2+} channels. *J Biol Chem* **273**, 13403–13406.

2 Lanner JT, Georgiou DK, Joshi AD & Hamilton SL (2010) Ryanodine receptors: structure, expression, molecular details, and function in calcium release. *Cold Spring Harb Perspect Biol* **2**, a003996.

3 MacLennan DH & Phillips MS (1992) Malignant hyperthermia. *Science* **256**, 789–794.

4 Loke J & MacLennan DH (1998) Malignant hyperthermia and central core disease: disorders of Ca^{2+} release channels. *Am J Med* **104**, 470–486.

5 MacLennan DH (2000) Ca^{2+} signalling and muscle disease. *Eur J Biochem* **267**, 5291–5297.

6 Inui M, Saito A & Fleischer S (1987) Isolation of the ryanodine receptor from cardiac sarcoplasmic reticulum and identity with the feet structures. *J Biol Chem* **262**, 15637–15642.

7 Imagawa T, Smith JS, Coronado R & Campbell KP (1987) Purified ryanodine receptor from skeletal muscle sarcoplasmic reticulum is the Ca^{2+}-permeable pore of the calcium release channel. *J Biol Chem* **262**, 16636–16643.

8 Lai FA, Erickson H, Block BA & Meissner G (1987) Evidence for a junctional feet–ryanodine receptor complex from sarcoplasmic reticulum. *Biochem Biophys Res Commun* **143**, 704–709.

9 Zorzato F, Fujii J, Otsu K, Phillips M, Green NM, Lai FA, Meissner G & MacLennan DH (1990) Molecular cloning of cDNA encoding human and rabbit forms of the Ca^{2+} release channel (ryanodine receptor) of skeletal muscle sarcoplasmic reticulum. *J Biol Chem* **265**, 2244–2256.

10 Suko J, Maurer-Fogy I, Plank B, Bertel O, Wyskovsky W, Hohenegger M & Hellmann G (1993) Phosphorylation of serine 2843 in ryanodine receptor-calcium release channel of skeletal muscle by cAMP-, cGMP- and CaM-dependent protein kinase. *Biochim Biophys Acta* **1175**, 193–206.

11 Ibarra M CA, Wu S, Murayama K, Minami N, Ichihara Y, Kikuchi H, Noguchi S, Hayashi YK, Ochiai R & Nishino I (2006) Malignant hyperthermia in Japan: mutation screening of the entire ryanodine receptor type 1 gene coding region by direct sequencing. *Anesthesiology* **104**, 1146–1154.

12 Robinson R, Carpenter D, Shaw M-A, Halsall J & Hopkins P (2006) Mutations in RYR1 in malignant hyperthermia and central core disease. *Hum Mutat* **27**, 977–989.

13 Serysheva II, Orlova EV, Chiu W, Sherman MB, Hamilton SL & Heel MV (1995) Electron cryomicroscopy and angular reconstitution used to visualize the skeletal muscle calcium release channel. *Nat Struct Mol Biol* **2**, 18–24.

14 Radermacher M, Rao V, Grassucci R, Frank J, Timerman AP, Fleischer S & Wagenknecht T (1994) Cryo-electron microscopy and three-dimensional reconstruction of the calcium release channel/ryanodine receptor from skeletal muscle. *J Cell Biol* **127**, 411–423.

15 Samso M, Wagenknecht T & Allen PD (2005) Internal structure and visualization of transmembrane domains of the RyR1 calcium release channel by cryo-EM. *Nat Struct Mol Biol* **12**, 539–544.

16 Samso M, Feng W, Pessah I & Allen PD (2009) Coordinated movement of cytoplasmic and transmembrane domains of RyR1 upon gating. *PLoS Biol* **7**, e1000085.

17 Amador FJ, Liu S, Ishiyama N, Plevin MJ, Wilson A, MacLennan DH & Ikura M (2009) Crystal structure of type I ryanodine receptor amino-terminal β-trefoil domain reveals a disease-associated mutation 'hot spot' loop. *Proc Natl Acad Sci USA* **106**, 11040–11044.

18 Tung C-C, Lobo PA, Kimlicka L & Van Petegem F (2010) The amino-terminal disease hotspot of ryanodine receptors forms a cytoplasmic vestibule. *Nature* **468**, 585–588.

19 Ryan T, Sharma P, Ignatchenko A, MacLennan DH, Kislinger T & Gramolini AO (2011) Identification of novel ryanodine receptor 1 (RyR1) protein interaction

with calcium homeostasis endoplasmic reticulum protein (CHERP). *J Biol Chem* **286**, 17060–17068.
20 Zhang L, Kelley J, Schmeisser G, Kobayashi YM & Jones LR (1997) Complex formation between junctin, triadin, calsequestrin, and the ryanodine receptor. *J Biol Chem* **272**, 23389–23397.
21 Brillantes A-MB, Ondrias K, Scott A, Kobrinsky E, Ondriasová E, Moschella MC, Jayaraman T, Landers M, Ehrlich BE & Marks AR (1994) Stabilization of calcium release channel (ryanodine receptor) function by FK506-binding protein. *Cell* **77**, 513–523.
22 Dolinski K & Botstein D (2007) Orthology and functional conservation in eukaryotes. *Annu Rev Genet* **41**, 465–507.
23 Sharma P, Nair U, Li W, Ryan T, Miyake T, Dong A, Kislinger T, Dhe-Paganon S & Gramolini A (2011) Comprehensive analysis of ryanodine receptor through proteomic interaction analysis and high resolution crystal structure determination. *Circulation* **124**, A15352.
24 Obenauer JC, Cantley LC & Yaffe MB (2003) Scansite 2.0: proteome-wide prediction of cell signaling interactions using short sequence motifs. *Nucleic Acids Res* **31**, 3635–3641.
25 Holm L, Kääriäinen S, Wilton C & Plewczynski D (2006) Using Dali for structural comparison of proteins. *Curr Protoc Bioinformatics* **14**, 5.5.1–5.5.24.
26 Wriggers W, Milligan RA & McCammon JA (1999) Situs: a package for docking crystal structures into low-resolution maps from electron microscopy. *J Struct Biol* **125**, 185–195.
27 Meng X, Xiao B, Cai S, Huang X, Li F, Bolstad J, Trujillo R, Airey J, Chen SR, Wagenknecht T, *et al.* (2007) Three-dimensional localization of serine 2808, a phosphorylation site in cardiac ryanodine receptor. *J Biol Chem* **282**, 25929–25939.
28 Jones P, Meng X, Xiao B, Cai S, Bolstad J, Wagenknecht T, Liu Z & Chen SRW (2008) Localization of PKA phosphorylation site, Ser^{2030}, in the three-dimensional structure of cardiac ryanodine receptor. *Biochem J* **410**, 261–270.
29 Yuchi Z, Lau K & Van Petegem F (2012) Disease mutations in the ryanodine receptor central region: crystal structures of a phosphorylation hot spot domain. *Structure* **20**, 1201–1211.
30 Hamilton SL & Serysheva II (2009) Ryanodine receptor structure: progress and challenges. *J Biol Chem* **284**, 4047–4051.
31 Galli L, Orrico A, Lorenzini S, Censini S, Falciani M, Covacci A, Tegazzin V & Sorrentino V (2006) Frequency and localization of mutations in the 106 exons of the RYR1 gene in 50 individuals with malignant hyperthermia. *Hum Mutat* **27**, 830.
32 Monnier N, Kozak-Ribbens G, Krivosic-Horber R, Nivoche Y, Qi D, Kraev N, Loke J, Sharma P, Tegazzin V, Figarella-Branger D, *et al.* (2005) Correlations between genotype and pharmacological, histological, functional, and clinical phenotypes in malignant hyperthermia susceptibility. *Hum Mutat* **26**, 413–425.
33 Zhou H, Jungbluth H, Sewry CA, Feng L, Bertini E, Bushby K, Straub V, Roper H, Rose MR, Brockington M, *et al.* (2007) Molecular mechanisms and phenotypic variation in RYR1-related congenital myopathies. *Brain* **130**, 2024–2036.
34 Bosanac I, Michikawa T, Mikoshiba K & Ikura M (2004) Structural insights into the regulatory mechanism of IP3 receptor. *Biochim Biophys Acta* **1742**, 89–102.
35 Berridge MJ (1993) Inositol trisphosphate and calcium signalling. *Nature* **361**, 315–325.
36 Seo M-D, Velamakanni S, Ishiyama N, Stathopulos PB, Rossi AM, Khan SA, Dale P, Li C, Ames JB, Ikura M, *et al.* (2012) Structural and functional conservation of key domains in InsP3 and ryanodine receptors. *Nature* **483**, 108–112.
37 Block BA, Imagawa T, Campbell KP & Franzini-Armstrong C (1988) Structural evidence for direct interaction between the molecular components of the transverse tubule/sarcoplasmic reticulum junction in skeletal muscle. *J Cell Biol* **107**, 2587–2600.
38 Pearson RB, Woodgett JR, Cohen P & Kemp BE (1985) Substrate specificity of a multifunctional calmodulin-dependent protein kinase. *J Biol Chem* **260**, 14471–14476.
39 White RR, Kwon Y-G, Taing M, Lawrence DS & Edelman AM (1998) Definition of optimal substrate recognition motifs of Ca^{2+}-calmodulin-dependent protein kinases IV and II reveals shared and distinctive features. *J Biol Chem* **273**, 3166–3172.
40 Westcott EB & Jackson WF (2011) Heterogeneous function of ryanodine receptors, but not IP3 receptors, in hamster cremaster muscle feed arteries and arterioles. *Am J Physiol* **300**, H1616–H1630.
41 Chu A, Sumbilla C, Inesi G, Jay SD & Campbell KP (1990) Specific association of calmodulin-dependent protein kinase and related substrates with the junctional sarcoplasmic reticulum of skeletal muscle. *Biochemistry* **29**, 5899–5905.
42 Wehrens XHT, Lehnart SE, Reiken SR & Marks AR (2004) Ca^{2+}/calmodulin-dependent protein kinase II phosphorylation regulates the cardiac ryanodine receptor. *Circ Res* **94**, e61–e70.
43 Said M, Becerra R, Valverde CA, Kaetzel MA, Dedman JR, Mundiña-Weilenmann C, Wehrens XH, Vittone L & Mattiazzi A (2011) Calcium–calmodulin dependent protein kinase II (CaMKII): a main signal responsible for early reperfusion arrhythmias. *J Mol Cell Cardiol* **51**, 936–944.
44 Pogwizd SM & Bers DM (2004) Cellular basis of triggered arrhythmias in heart failure. *Trends Cardiovasc Med* **14**, 61–66.

45 van Oort RJ, McCauley MD, Dixit SS, Pereira L, Yang Y, Respress JL, Wang Q, De Almeida AC, Skapura DG, Anderson ME, *et al*. (2010) Ryanodine receptor phosphorylation by calcium/calmodulin-dependent protein kinase II promotes life-threatening ventricular arrhythmias in mice with heart failure. *Circulation* **122**, 2669–2679.
46 Farr MA & Basson CT (2004) Sparking the failing heart. *New Engl J Med* **351**, 185–187.
47 Dobrev D & Wehrens XHT (2010) Calmodulin kinase II, sarcoplasmic reticulum Ca^{2+} leak, and atrial fibrillation. *Trends Cardiovasc Med* **20**, 30–34.
48 Alenkin D, Yermekbayeva L, Mujib S, Vesterberg A, Newman E, Yamazaki K, Cossar D & Dhe-Paganon S (2011) A centrifugation-free high-throughput protein purification system using in-line microfluidization. *Protein Expr Purif* **79**, 204–209.
49 Minor W, Cymborowski M, Otwinowski Z & Chruszcz M (2006) HKL-3000: the integration of data reduction and structure solution – from diffraction images to an initial model in minutes. *Acta Crystallogr D Biol Crystallogr* **62**, 859–866.
50 Sheldrick GM (2008) A short history of SHELX. *Acta Crystallogr A* **64**, 112–122.
51 Terwilliger TC & Berendzen J (1999) Automated MAD and MIR structure solution. *Acta Crystallogr D Biol Crystallogr* **55**, 849–861.
52 Terwilliger T (2003) Automated main-chain model building by template matching and iterative fragment extension. *Acta Crystallogr D Biol Crystallogr* **59**, 38–44.
53 Emsley P & Cowtan K (2004) Coot: model-building tools for molecular graphics. *Acta Crystallogr D Biol Crystallogr* **60**, 2126–2132.
54 Bricogne G, Blanc E, Brandl M, Flensburg C, Keller P, Paciorek W, Roversi P, Smart OS, Vonrhein C & Womack TO (2009) BUSTER, Version 2.8.0. Global Phasing Ltd, Cambridge, UK.
55 Pettersen EF, Goddard TD, Huang CC, Couch GS, Greenblatt DM, Meng EC & Ferrin TE (2004) UCSF Chimera – a visualization system for exploratory research and analysis. *J Comput Chem* **25**, 1605–1612.
56 Brini M, Manni S, Pierobon N, Du GG, Sharma P, MacLennan DH & Carafoli E (2005) Ca^{2+} signaling in HEK-293 and skeletal muscle cells expressing recombinant ryanodine receptors harboring malignant hyperthermia and central core disease mutations. *J Biol Chem* **280**, 15380–15389.

Supporting information

The following supplementary material is available:
Fig. S1. C3 construct sequence analysis.
Fig. S2. Placement of the RyR domain into the cryo-EM maps of RyR.
Fig. S3. C3 construct sequence analysis between RyR1 and RyR2.
Table S1. Diffraction data, processing and structure refinement statistics.
Table S2. CaMKIIβ peptides found in each mass spectrometry run for RyR1 C1–C3 constructs.
Movie S1. Dynamic movements of the RyR1 during channel opening and closing.

This supplementary material can be found in the online version of this article.

Please note: As a service to our authors and readers, this journal provides supporting information supplied by the authors. Such materials are peer-reviewed and may be reorganized for online delivery, but are not copy-edited or typeset. Technical support issues arising from supporting information (other than missing files) should be addressed to the authors.